

# Neurophotonics

Neurophotonics.SPIEDigitalLibrary.org

## **Nanoscale organization of synaptic adhesion proteins revealed by single-molecule localization microscopy**

Ingrid Chamma  
Florian Levet  
Jean-Baptiste Sibarita  
Matthieu Sainlos  
Olivier Thoumine

# Nanoscale organization of synaptic adhesion proteins revealed by single-molecule localization microscopy

Ingrid Chamma,<sup>a,b</sup> Florian Levet,<sup>a,b,c,d,e</sup> Jean-Baptiste Sibarita,<sup>a,b</sup> Matthieu Sainlos,<sup>a,b</sup> and Olivier Thoumine<sup>a,b,\*</sup>

<sup>a</sup>Centre National de la Recherche Scientifique, Interdisciplinary Institute for Neuroscience, UMR 5297, 147 rue Léo-Saignat, Bordeaux Cedex 33077, France

<sup>b</sup>University of Bordeaux, Interdisciplinary Institute for Neuroscience, 147 rue Léo-Saignat, Bordeaux Cedex 33077, France

<sup>c</sup>Centre National de la Recherche Scientifique, Bordeaux Imaging Center, UMS 3420, Bordeaux 33077, France

<sup>d</sup>University of Bordeaux, Bordeaux Imaging Center, Bordeaux 33077, France

<sup>e</sup>Institut National de la Santé et de la Recherche Médicale, Bordeaux Imaging Center, US 04, Bordeaux 33077, France

**Abstract.** The advent of superresolution imaging has created a strong need for both optimized labeling strategies and analysis methods to probe the nanoscale organization of complex biological structures. We present a thorough description of the distribution of synaptic adhesion proteins at the nanoscopic scale, namely presynaptic neurexin-1 $\beta$  (Nrx1 $\beta$ ), and its two postsynaptic binding partners neuroligin-1 (Nlg1) and leucine-rich-repeat transmembrane protein 2 (LRRTM2). We monitored these proteins in the membrane of neurons by direct stochastic optical reconstruction microscopy, after live surface labeling with Alexa647-conjugated monomeric streptavidin. The small probe ( $\sim$ 3 nm) efficiently penetrates into crowded synaptic junctions and reduces the distance to target. We quantified the organization of the single-molecule localization data using a tessellation-based analysis technique. We show that Nlg1 exhibits a fairly disperse organization within dendritic spines, while LRRTM2 is organized in compact domains, and Nrx1 $\beta$  in presynaptic terminals displays a dual-organization pattern intermediate between that of Nlg1 and LRRTM2. These results suggest that part of Nrx1 $\beta$  interacts transsynaptically with Nlg1 and the other part with LRRTM2. © 2016 Society of Photo-Optical Instrumentation Engineers (SPIE) [DOI: 10.1117/1.NPh.3.4.041810]

Keywords: superresolution; synapse; adhesion proteins; direct stochastic optical reconstruction microscopy; SR-Tesseler.

Paper 16046SSR received Jul. 4, 2016; accepted for publication Oct. 11, 2016; published online Nov. 3, 2016.

## 1 Introduction

Synaptic contacts are dynamic macromolecular platforms with extreme spatial and temporal coordination allowing information transfer between neurons. The efficiency of synaptic transmission relies in part on a high level of compartmentation. Indeed, synapses are composed of several subdomains with very high local protein concentration including the cytomatrix active zone, the synaptic cleft, and the postsynaptic density. Single-molecule-based localization microscopy techniques, including photoactivation localization microscopy (PALM),<sup>1,2</sup> stochastic optical reconstruction microscopy (STORM),<sup>3,4</sup> and point accumulation for imaging in nanoscale topography (PAINT),<sup>5,6</sup> have provided high-resolution maps of synaptic protein localization, allowing a better understanding of the organization of these submicron multisubunit assemblies.<sup>7–12</sup> Adhesion molecules such as neuexins (Nrxs) and its binding partners neuroligins (Nlgs) and leucine-rich repeat transmembrane proteins (LRRTMs) are important actors at synapses, not only maintaining a physical contact between pre- and postsynaptic membranes, but also participating in synapse formation, differentiation, and activity.<sup>13–15</sup>

In the absence of high-quality antibodies for surface labeling of Nlgs and LRRTMs, we recently developed a method based on streptavidin monomers (mSA)<sup>16</sup> to deliver bright organic fluorophores to proteins that are enzymatically biotinylated on a

15 amino acid acceptor peptide (AP) tag.<sup>17</sup> We used this technique to label neuroligin-1 (Nlg1) and leucine-rich-repeat transmembrane protein 2 (LRRTM2) at postsynapses by direct STORM (dSTORM) and demonstrated the different nanoscale organization of these two proteins, which may underlie divergent physiological roles at the synapse.<sup>18</sup> In addition, we and others previously showed by using single-particle tracking that neurexin-1 $\beta$  (Nrx1 $\beta$ ) diffuses relatively quickly in the axonal membrane and accumulates transiently at presynapses,<sup>18,19</sup> but the precise nanoscale organization of Nrx1 $\beta$  within presynaptic terminals remains undescribed. However, deciphering the spatial distribution of Nrx is important to understand the interplay between the presynaptic release machinery and synaptic cleft components, especially given the dramatic impact of Nrx knock-out on synaptic transmission.<sup>20</sup> Furthermore, given that Nrx1 $\beta$  can bind to Nlg1 and LRRTM2 in a competitive manner and with similar affinity,<sup>21–23</sup> it would be interesting to know if Nrx1 $\beta$  has a preferential transsynaptic interacting partner.

In this paper, we use the mSA strategy to label Nrx1 $\beta$  molecules at presynapses in combination with dSTORM and SR-Tesseler, a tessellation-based analysis technique,<sup>24</sup> to quantify the local protein organization of Nrx1 $\beta$ , Nlg1, and LRRTM2 within synapses. We show that Nlg1 exhibits a rather disperse organization in dendritic spines, while LRRTM2 is organized in

\*Address all correspondence to: Olivier Thoumine, E-mail: [olivier.thoumine@u-bordeaux.fr](mailto:olivier.thoumine@u-bordeaux.fr)

compact and highly enriched domains. Interestingly, *Nrx1 $\beta$*  in presynaptic terminals displays both a diffuse organization resembling that of *Nlg1* and well-defined clusters reminiscent of the *LRRTM2* organization, suggesting that *Nrx1 $\beta$*  interacts independently with both partners at synapses.

## 2 Results

### 2.1 Nanoscale Organization of *Nrx1 $\beta$* at Presynapses

To image *Nrx* at presynapses, primary rat hippocampal neurons were electroporated at the time of plating (day *in vitro* DIV 0) with a *Nrx1 $\beta$*  construct carrying a 15 amino acid *N*-terminal biotin acceptor peptide (AP) tag (AP-*Nrx1 $\beta$* ), together with the endoplasmic reticulum-resident biotin ligase (BirA<sup>ER</sup>),<sup>17</sup> and a VGlut1-Super Ecliptic (SEP) presynaptic reporter. Biotin naturally present in the culture medium is covalently added to a central lysine residue in the AP-tag through the enzymatic action of the biotin ligase, and AP-*Nrx1 $\beta$*  reaches the plasma membrane in a biotinylated form.<sup>25</sup> The biotinylated

tag is then detected by incubation with monomeric streptavidin (mSA) conjugated to an organic dye (Alexa647), compatible with dSTORM. In DIV 15 neurons, we observed an excellent colocalization of the Alexa647 mSA conjugate with VGlut1-SEP [Fig. 1(a)], indicating that mSA-labeled AP-*Nrx1 $\beta$*  efficiently reaches presynapses. The axonal shaft was almost depleted of staining, probably owing to the fast diffusion of *Nrx1 $\beta$*  in this compartment.<sup>18,19</sup> Zooming on presynapses to decipher the internal substructure of *Nrx1 $\beta$*  distribution, we found that *Nrx1 $\beta$*  exhibits a dual-localization pattern: one population fairly dispersed within the presynaptic membrane and a second population condensed into 1 to 2 nanocluster(s) (mean  $1.4 \pm 0.18$ , 24 synapses) with higher protein density [Figs. 1(b), 1(c), 1(d)]. Using the SR-Tesseler segmentation technique,<sup>24</sup> we determined the size of those nanoclusters, which lays in the range of 50 to 200 nm (median  $118 \text{ nm} \pm \text{IQR } 80 \text{ to } 154 \text{ nm}$ , 37 synapses) [Fig. 1(e)]. These nanoclusters match the size of confinement domains previously observed by uPAINT performed on green fluorescent protein (GFP)-*Nrx1 $\beta$*  labeled with Atto647N-conjugated anti-GFP nanobody,<sup>18</sup> which most likely correspond to *Nrx1 $\beta$*  being trapped at presynapses.

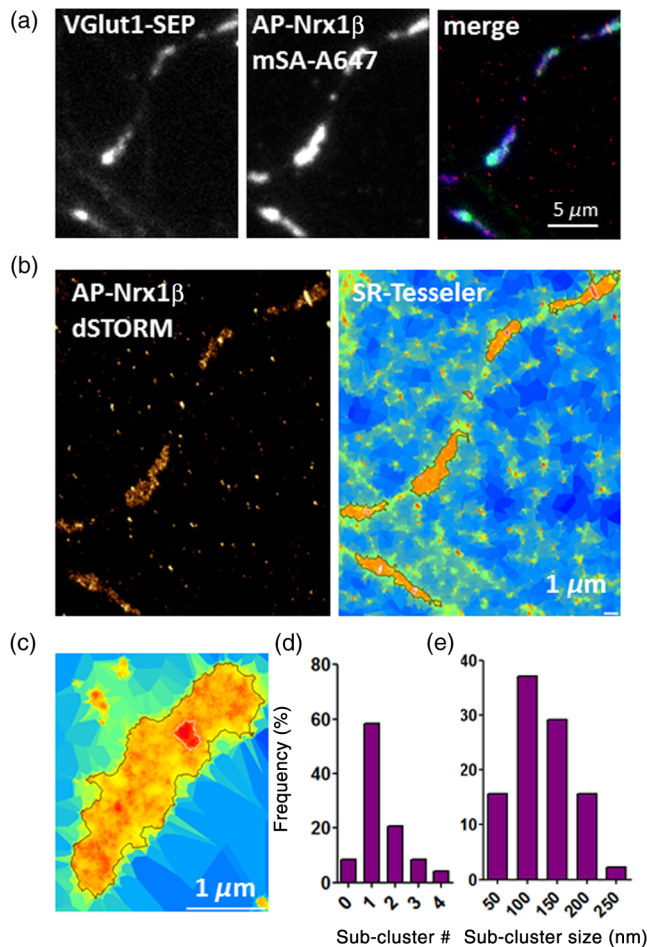


**Fig. 1** Nanoscale organization of *Nrx1 $\beta$*  at the presynapse. (a) DIV 15 neurons expressing the presynaptic marker VGlut1-SEP, AP-*Nrx1 $\beta$* , and BirA<sup>ER</sup> were labeled with mSA-Alexa647 and fixed for dSTORM. (b) dSTORM image of an axonal segment with four presynapses and corresponding Voronoi diagram showing *Nrx1 $\beta$*  enrichment at presynapses, as well as subcluster formation within these enriched regions. (c) Zoom on an *Nrx1 $\beta$*  subcluster in the polygon representation. (d) Number of *Nrx1 $\beta$*  subclusters per presynapse. (e) Histogram showing the sizes of *Nrx1 $\beta$*  subclusters.

### 2.2 Difference of Organization Between *Nrx1 $\beta$* , *Nlg1*, and *LRRTM2* at Synapses

To gain insight on the nanoscale organization of postsynaptic adhesion proteins, we imaged *Nlg1* and *LRRTM2* by dSTORM in DIV 15 neurons (Fig. 2). *Nlg1* was both present in the shaft and mildly enriched in dendritic spines, where it exhibited a fairly homogeneous distribution [Fig. 2(a)]. In contrast, *LRRTM2* was almost depleted from the shaft and highly enriched in dendritic spines, where it formed one main central cluster with higher protein density [Fig. 2(b)]. To compare the nanoscale organization of *Nlg1* and *LRRTM2*, we used SR-Tesseler<sup>24</sup> to define a local molecular density parameter  $d$  expressed in a log scale. For *Nlg1*, the distribution of molecule density exhibited a single population [Fig. 2(d)], reflecting the fact that *Nlg1* covers a continuum of organizational states, from a very diffuse state in the shaft to the formation of small synaptic and extrasynaptic aggregates.<sup>18</sup> In contrast, the  $d$  distribution for *LRRTM2* was broader and composed of two populations [Fig. 2(e)]: a first population of lower density revealing a relative depletion of *LRRTM2* from the shaft compared to synapses and a second population of much higher protein density, likely corresponding to the highly enriched synaptic *LRRTM2* domains.<sup>18</sup> Interestingly, when applying the same method to presynapses, *Nrx1 $\beta$*  also showed a bimodal  $d$  distribution [Fig. 2(f)], with a first large peak of lower density likely representing *Nrx1 $\beta$*  present in the axon shaft and at presynapses, and a second peak much shifted to the right, matching the enriched protein density in nanoclusters [Fig. 2(c)]. Altogether, these results suggest that *Nrx1 $\beta$*  displays two modes of organization: a diffuse state resembling *Nlg1* organization and a concentrated state reminiscent of *LRRTM2* or even more enriched.

### 2.3 *Nrx1 $\beta$* Organizational Patterns Display Close Similarities to Both *Nlg1* and *LRRTM2*

To compare the nanoscale organization of presynaptic *Nrx1 $\beta$*  facing that of postsynaptic *Nlg1* and *LRRTM2*, we defined the enrichment factor  $R$ , which measures the normalized molecular concentration on a linear scale. This enrichment factor was then

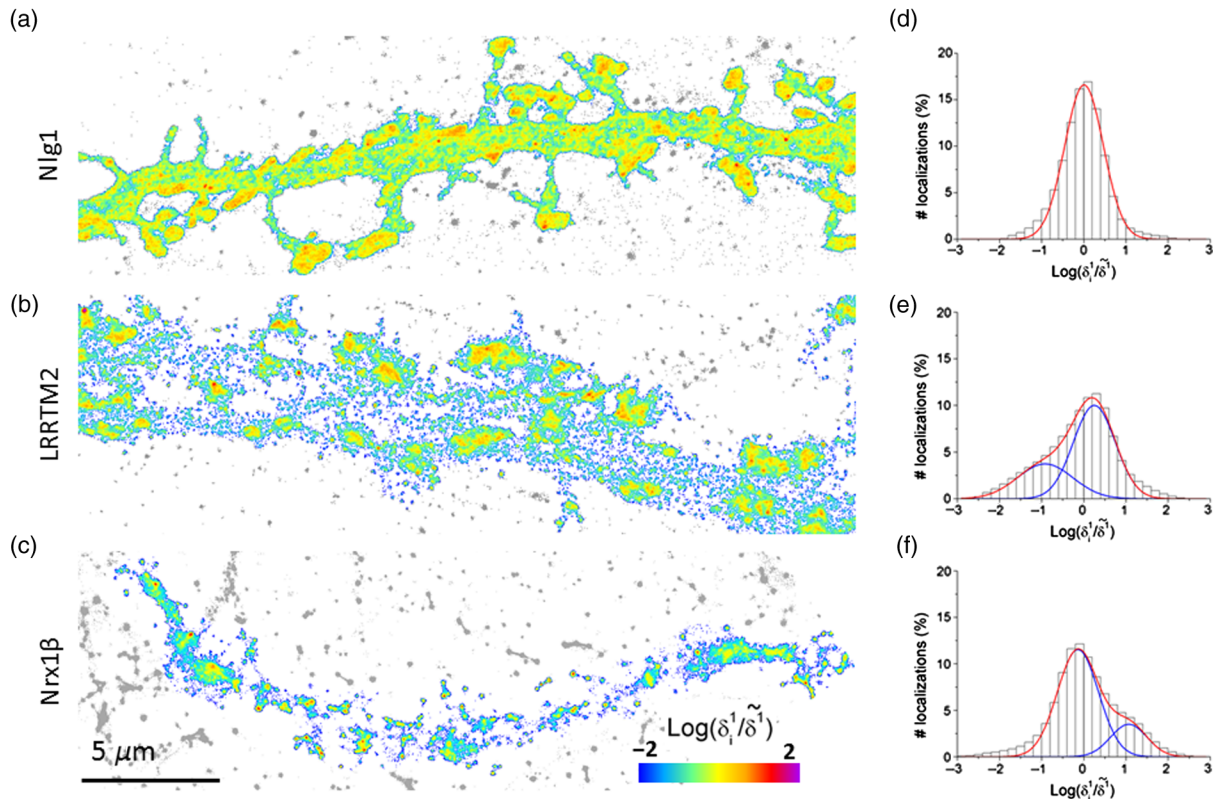


**Fig. 2** Differential organization of Nrx1 $\beta$ , Nlg1, and LRRTM2 in synaptic compartments. (a, c, and e) Color-coded images showing the normalized molecular densities in log scale for (a) Nlg1, (b) LRRTM2, and (c) Nrx1 $\beta$  obtained from dSTORM images of AP-tagged proteins labeled with mSA-Alexa647. Note the relatively homogenous localization of Nlg1 (green and yellow values) throughout the shaft and dendritic spines, as compared to Nrx1 $\beta$  and LRRTM2 which are highly segregated in pre- and postsynaptic compartments, respectively (blue in the shaft and red in synapses). (d, e, and f) Corresponding distributions of the relative molecular density in semilog plot for Nlg1, LRRTM2, and Nrx1 $\beta$ . Statistics: Nlg1 (3 cells, 3,653,239 localizations,  $R^2 = 0,998$ ), LRRTM2 (5 cells, 2,971,150 localizations,  $R^2 = 0,992$ ), and Nrx1 $\beta$  (5 cells, 1,582,629 localizations,  $R^2 = 0,988$ ). Note the single population for Nlg1, and the dual populations for LRRTM2 and Nrx1 $\beta$ .

used as a threshold to highlight the enriched areas with respect to nonenriched ones [Fig. 3(a)].

We then graphed two parameters as a function of  $R$ : the fraction of neuronal area occupied by enriched regions  $A(R)$  [Fig. 3(b)] and the fraction of the number of localizations inside those enriched regions  $N(R)$  [Fig. 3(c)]. Interestingly,  $A(R)$  was significantly lower for LRRTM2 than for Nlg1, confirming that LRRTM2 is segregated in smaller regions in the spines than Nlg1. When  $A(R)$  becomes equivalent for Nlg1 and LRRTM2 for higher  $R$  [Fig. 3(b)],  $N(R)$  remains two- to threefold higher for LRRTM2 compared to Nlg1 [Fig. 3(c)], indicating that these LRRTM2 segregated regions are much denser.

On the other hand, the curve  $A(R)$  for Nrx1 $\beta$  is situated between those of Nlg1 and LRRTM2.  $A(R)$  falls deeper than the curve corresponding to Nlg1 due to the fact that the diffuse Nrx1 $\beta$  population covers a relatively small presynaptic surface area compared to Nlg1. In parallel, the curve  $A(R)$  for Nrx1 $\beta$  remains higher than that of LRRTM2, because LRRTM2 is segregated in small regions in the spines and lacks a diffuse population. Finally, while Nrx1 $\beta$  is slightly more concentrated than LRRTM2 for low  $R$ ,  $N(R)$  becomes equivalent for large  $R$ . This suggests that Nrx1 $\beta$  has a dual organization, one part being fairly diffuse and disappearing when reaching intermediate  $R$  and the other more concentrated with a magnitude equivalent to LRRTM2.

### 3 Discussion

Using quantitative localization-based superresolution microscopy, we unraveled for the first time the relative distribution of presynaptic Nrx1 $\beta$  and its postsynaptic binding partners Nlg1 and LRRTM2 in primary hippocampal neurons. We implemented a pipeline combining high density labeling with small photo-robust monomeric probes, allowing accurate localization in synaptic compartments, with a dedicated polygon-based analysis of single-molecule localizations distribution obtained by dSTORM. This analysis allowed the calculation of protein concentration gradients, going much beyond traditional approaches based on intensity line scans to determine protein enrichment.<sup>24</sup> We demonstrate that Nrx1 $\beta$  exhibits a dual distribution, comprising a diffuse presynaptic component that matches the distribution of postsynaptic Nlg1, plus 1 to 2 compact nanoclusters enriched in a similar way compared to LRRTM2 domains. This suggests that one population of Nrx1 $\beta$  molecules may diffuse alone or could be transsynaptically linked to Nlg1 as small molecular complexes, while another population of Nrx1 $\beta$  may be aggregated in connection to large LRRTM2 domains. The fact that Nrx1 $\beta$  cannot simultaneously bind Nlg1 and LRRTM2<sup>21,26</sup> suggests that these two types of distributions are mutually exclusive. Based on our previous dual-color uPAINT experiments on Nrx1 $\beta$  versus Nlg1 or

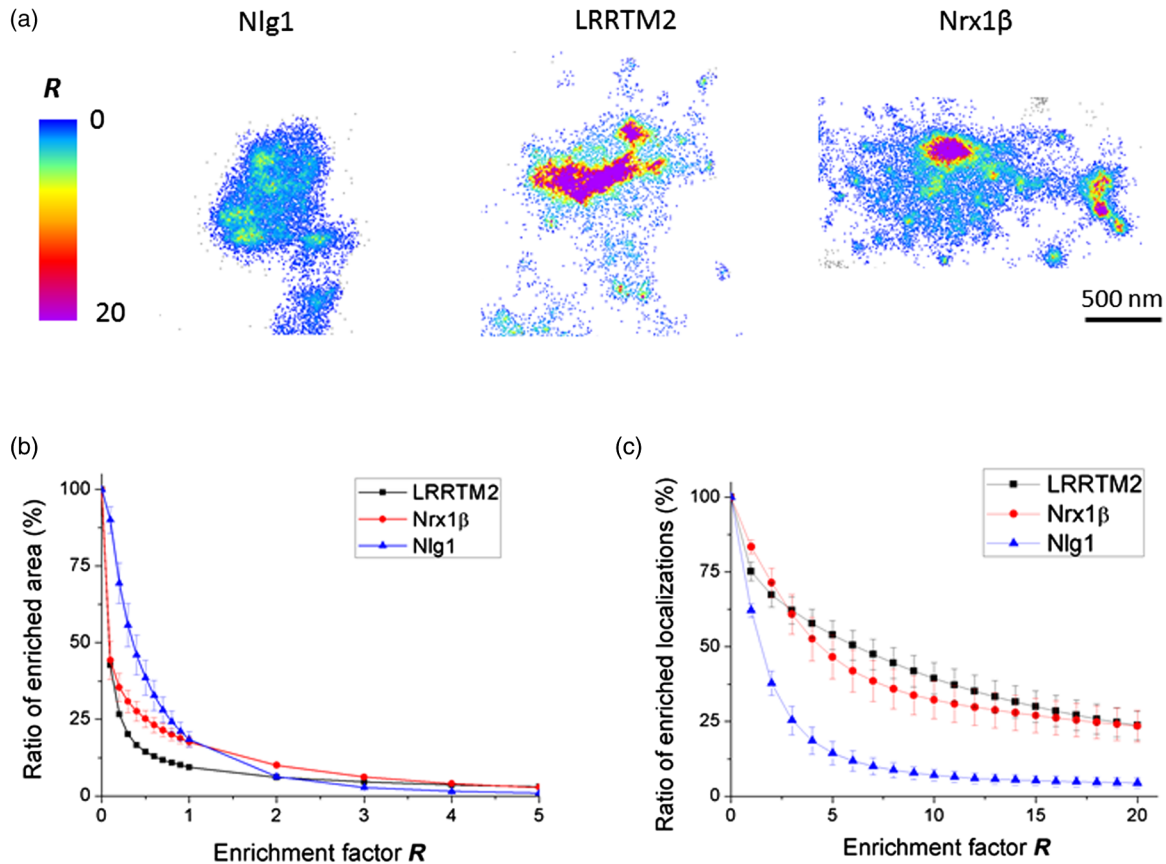


**Fig. 3** The nanoscale organization of Nr1 $\beta$  lies between that of Nlg1 and LRRTM2. (a) Color-coded images showing the enrichment factor  $R$  in linear scale for Nlg1, LRRTM2 in two dendritic spines, and Nr1 $\beta$  in a presynaptic terminal. Note the mild synaptic enrichment of Nlg1 compared to LRRTM2, which is highly concentrated in a single large domain. Nr1 $\beta$  shows both a diffuse distribution throughout the presynapse, together with small and highly enriched nanoclusters. (b) Ratio of the enriched area relative to the whole neuronal area considered  $A(R)$ , as a function of the enrichment factor  $R$ , for the three proteins.  $A(R)$  drops quickly as the enrichment factor is increased, and the curve for Nr1 $\beta$  lies between those representing Nlg1 and LRRTM2. (c) Ratio of the number of single-molecule localizations in enriched areas  $N(R)$ , relative to the total number of localizations in the neuronal area, as a function of the enrichment factor  $R$ , for the three proteins. In this quantification, the curve for Nr1 $\beta$  is closer to that of LRRTM2.

LRRTM2,<sup>18</sup> we expect the homogeneously distributed Nr1 $\beta$  and Nlg1 population to represent dynamic complexes that exhibit fast diffusion in the shaft and are transiently trapped at synapses,<sup>18,19</sup> while the Nr1 $\beta$ /LRRTM2 clusters at the core of the synaptic cleft are predicted to be much more stable. This simple picture might become a little more complex if we consider that all these molecules exist as different isoforms and splice variants, e.g., Nlg1 and LRRTM2 might also interact with  $\alpha$ -Nrxs present at the presynapse.<sup>19</sup>

In the absence of high-quality antibodies against surface epitopes on endogenous Nr1, Nlg, or LRRTM2, we monitored the distribution of recombinant AP-tagged proteins. Thus, local molecular densities should not be interpreted as absolute values quantitatively reflecting the behavior of endogenous proteins, but as relative measurements allowing comparison of the distribution of the three synaptic adhesion proteins. Nevertheless, to avoid massive overexpression of proteins that could bias their intrinsic localization, we transfected neurons through electroporation with very low deoxyribose nucleic acid (DNA) amounts. In this context, we previously quantified for Nlg1 that there was roughly one exogenous molecule for one endogenous molecule,<sup>18</sup> and this ratio is likely to be more or less conserved for

Nr1 $\beta$  and LRRTM2, depending on endogenous protein levels and recombinant expression vectors. Furthermore, by replacing endogenous Nlg1 by recombinant AP-tagged Nlg1 using a knock-down plus rescue strategy, we obtained a similarly synaptic distribution of Nlg1 by STORM,<sup>18</sup> ruling out potential overexpression artifacts. A similar replacement approach could be used in the future for Nr1 $\beta$  and LRRTM2. To study the nanoscale organization of those proteins, monomeric ligands, such as mSA, provide a strong advantage over divalent antibodies or multivalent streptavidin in that they do not induce cross-linking or the formation of artificial nanoclusters, which would otherwise bias the measurements.<sup>17,18</sup>

Our approach was based on the comparative statistical analysis of the distribution of individual synaptic components, imaged one at a time. However, in order to unambiguously identify the one-to-one association between presynaptic Nr1 $\beta$  substructures and the ones corresponding to Nlg1 or LRRTM2, it would be interesting to setup a dual or triple color imaging configuration of those synaptic adhesion molecules. To this aim, one would need orthogonal labeling strategies to discriminate Nr1 $\beta$ , Nlg1, and LRRTM2. One difficulty is that Nlg1 and LRRTM2 do not tolerate well large extracellular or intracellular

tags that can perturb either adhesion to Nrxs,<sup>27</sup> or binding to scaffolding molecules such as PSD-95.<sup>28</sup> Thus, one would need instead to find a strategy relying on small extracellular tags. It will also be important to localize Nrxs, Nlgs, and LRRTMs with respect to other adhesion proteins of the synaptic cleft, in particular SynCAMs<sup>11</sup> and N-cadherin.<sup>29–31</sup>

The development of such multicolor superresolution imaging will enable us to establish a mapping of the distribution of adhesion proteins in relation to other important actors of the synapse, in particular scaffolding molecules and neurotransmitter receptors,<sup>9,32</sup> and their potential reshaping during synaptic plasticity. For example, we previously showed that the chemical induction of long-term depression in neuronal cultures by transient application of *N*-methyl-D-aspartate (NMDA) caused a progressive disappearance of both Nr1 $\beta$  and Nlg1 from the neuronal surface,<sup>18</sup> potentially through the cleavage of Nlg1 extracellular domain by the protease MMP9.<sup>33,34</sup> An extrasynaptic relocalization of SynCAM1 was also reported in response to NMDA treatment.<sup>11</sup> It would thus be interesting to assess whether there is a similar reorganization of LRRTM2 at synapses in relationship to presynaptic Nr1. Finally, it will be important to implement localization-based superresolution imaging methods in organotypic tissue where synaptic connectivity is preserved compared to dissociated cultures, so as to be able to apply well-established synaptic plasticity protocols.<sup>3,35</sup>

## 4 Methods

### 4.1 Deoxyribose Nucleic Acid Plasmids

The AP-Nlg1, AP-Nrx1 $\beta$ , and BirA<sup>ER</sup> constructs<sup>17,27</sup> were kind gifts from A. Ting (MIT, Boston). AP-LRRTM2 was generated using the In-Fusion HD Cloning kit (Clontech), replacing the myc-tag from myc-LRRTM2<sup>26</sup> (J. de Wit, Leuven, Belgium) by the AP-Tag (amino acid sequence GLNDIFEAQKIEWHE) as described.<sup>18</sup> SEP-VGlut1 was a kind gift from D. Perrais (Interdisciplinary Institute for Neuroscience, Bordeaux). mSA was subcloned from the previously described pRSET-A vector generously given by S. Park (Buffalo University, New York)<sup>36,37</sup> into pET-IG, a homemade vector derived from pET-24 (Novagen) and engineered to incorporate after the start codon a decahistidine tag immediately followed by a Tobacco Etch Virus cleavage site (-ENLYFQS-) and no tag on the C-terminus.

### 4.2 Streptavidin Monomers Production and Coupling to Fluorophores

mSA was produced as previously described.<sup>18</sup> Briefly, mSA, encoded in the pET-IG-mSA vector, was expressed by autoinduction in *Escherichia coli* BL21 codon plus<sup>TM</sup> (DE3)-RIL for 12 h at 16°C. Following lysis of the bacteria in denaturing conditions, the protein was purified by immobilized metal ion affinity chromatography with HIS-Buster Cobalt Affinity gel (AMOCOL) and refolded in presence of reduced and oxidized glutathione. The refolded protein was concentrated and coupled to Alexa Fluor 647 NHS ester following the recommended procedures from the manufacturer. Excess dye was removed using Sephadex G-25 medium, the conjugate was further purified to homogeneity by size exclusion chromatography, and the labeled protein was aliquoted and stored at -80°C until use.

### 4.3 Cell Culture and Electroporation

Pregnant female rats were purchased weekly (Janvier Labs, Saint-Berthevin, France). Animals were handled and euthanized according to European ethical rules. Dissociated hippocampal neurons from E18 Sprague-Dawley rats embryos were prepared as described<sup>38</sup> and electroporated with the Amaxa system (Lonza), using 500,000 cells per cuvette. The following plasmid combinations were used: (GFP or SEP-VGlut1) + BirA<sup>ER</sup> + (AP-Nlg1, AP-LRRTM2, or AP-Nrx1 $\beta$ ) (1.5:1.5:1.5)  $\mu$ g DNA. Electroporated neurons were resuspended in minimal essential medium supplemented with 10% horse serum (MEM-HS) and plated on 18-mm coverslips previously coated with 1 mg ml<sup>-1</sup> polylysine for 2 h, at a concentration of 50,000 cells per coverslip. Three hours after plating, coverslips were flipped onto 60-mm dishes containing a glial cell layer in neurobasal medium supplemented with 2 mM L-glutamine and 1 $\times$  NeuroCult SM1 Neuronal supplement (STEMCELL technologies), and cultured for 2 weeks at 37°C and 5% CO<sub>2</sub>. Astrocytes feeder layers were prepared from the same embryos, plated between 20,000 and 40,000 cells per 60-mm dish and cultured in MEM (Fisher Scientific, Cat. No. 21090-022) containing 4.5 g l<sup>-1</sup> glucose, 2-mM L-glutamine, and 10% horse serum (Invitrogen) for 14 days.

### 4.4 Direct Stochastic Optical Reconstruction Microscopy

Primary cultured neurons expressing AP-Nlg1, AP-LRRTM2, or AP-Nrx1 $\beta$  were surface-labeled with a high concentration (100 nM) of mSA-Alexa647 in Tyrode solution (15 mM D-glucose, 108 mM NaCl, 5 mM KCl, 2 mM MgCl<sub>2</sub>, 2 mM CaCl<sub>2</sub>, and 25 mM HEPES, pH 7.4) containing 1% globulin-free BSA (Sigma) for 10 min, rinsed and fixed with 4% PFA-0.2% glutaraldehyde in PBS for 10 min at room temperature. Before dSTORM acquisitions, the samples were incubated in a solution of PBS containing 1:1000 fluorescent beads (Tetraspec) used as markers for image registration. dSTORM imaging of cultured neurons was performed using an inverted motorized microscope (Nikon Ti-Eclipse, Japan) equipped with a 100 $\times$ /1.49 NA PL-APO objective and a perfect focus system, allowing long acquisition in oblique illumination mode. Both the ensemble and single-molecule fluorescence were collected by using a quad-band dichroic filter (Di01-R405/488/561/635, Semrock, New York). The fluorescence was collected using a sensitive EMCCD (Evolve, Photometrics, Arizona). Single-molecule localization and reconstruction were performed online with automatic feedback control of the lasers using WaveTracer module, enabling optimal single-molecule density during the acquisition.<sup>39</sup> The acquisition and localization sequences were driven by MetaMorph software (Molecular Devices, California) in streaming mode at 50 frames/s (20-ms exposure time) using an area equal to or less than a 256 $\times$ 256 pixels region of interest. dSTORM superresolution images were reconstructed from 40,000 frames.

### 4.5 Image Reconstruction and Analysis

Image stacks were analyzed using a custom plugin running on MetaMorph software based on wavelet segmentation.<sup>39,40</sup> It allows reconstructing the superresolution images by summing the positions of localized single molecules into a single image and exporting files containing the spatial coordinates of each

localization. Fluorescent beads (Tetraspec) were used as fiducial markers for image registration.

#### 4.6 Protein Quantification Using Tessellation-Based Analysis

We used SR-Tesseler<sup>24</sup> to quantify the molecular organization of the three synaptic adhesion proteins. Single-molecule localization coordinates were used to compute a Voronoi tessellation in order to partition the image space in polygons of various sizes centered on each localized molecule. Using this space-partitioning framework, first-rank densities  $\delta_i^1$  of the molecules were computed<sup>24</sup> and density maps were generated by texturing the Voronoi polygons with  $\delta_i^1$  values. Segmentations of the mSA-labeled AP-Nrx1 $\beta$  presynapses were performed by applying a threshold of twice the average density  $\delta$  of the whole axonal region. Then subcluster organization of the Nrx1 $\beta$  distribution was obtained by applying a threshold of twice the average density of each presynapse. All selected neighboring molecules were merged together to segment presynapses and subclusters, and the size parameters were extracted by principal component analysis.

To determine the nanoscale organization of the three proteins, we first segmented the diffracted-limited low-resolution images using intensity-based thresholding in MetaMorph software. The neuronal regions  $N$  were identified by segmenting the localizations inside those masks. All subsequent analyses were performed exclusively on the localizations belonging to  $N$ . For each protein, normalization of the density distribution was achieved by dividing the density  $\delta_i^1$  of each molecule by the median  $\tilde{\delta}^1$  of all  $\delta_i^1$ . The enrichment factor  $R$  was defined as the ratio between the molecule density  $\delta_i^1$  and the average density  $\delta^N$  of the neuronal region. By varying  $R$  (from 0 to 20), we determined enriched regions (for  $R > 0$ ) with a given area  $A(R)$  and a number of localization  $N(R)$ .  $A(R)$  reflects the surface occupation for  $\delta_i^1 \geq R \times \delta^N$  and  $N(R)$  the number of localizations within this area.

#### Acknowledgments

We thank A. Ting and S. Park for the generous gift of DNA plasmids, B. Tessier for molecular biology, the Cell Culture Facility of the Institute (especially E. Verdier and P. Durand), and J. Gilardin for technical support. This work received funding from the Centre National de la Recherche Scientifique, Agence Nationale pour la Recherche (grants Synapse-2Dt, Nanodom, and SynAdh), Conseil Régional Aquitaine, Investissements d'Avenir Labex BRAIN, Fondation pour la Recherche Médicale, and the National Infrastructure France BioImaging (Grant No. ANR-10INBS-04-01).

#### References

1. S. Manley et al., "High-density mapping of single-molecule trajectories with photoactivated localization microscopy," *Nat. Methods* **5**(2), 155–157 (2008).
2. H. Shroff et al., "Live-cell photoactivated localization microscopy of nanoscale adhesion dynamics," *Nat. Methods* **5**(5), 417–423 (2008).
3. A. Dani et al., "Superresolution imaging of chemical synapses in the brain," *Neuron* **68**(5), 843–856 (2010).
4. M. Heilemann et al., "Subdiffraction-resolution fluorescence imaging with conventional fluorescent probes," *Angew. Chemie—Int. Ed.* **47**(33), 6172–6176 (2008).
5. A. Sharonov and R. M. Hochstrasser, "Wide-field subdiffraction imaging by accumulated binding of diffusing probes," *Proc. Natl. Acad. Sci. U. S. A.* **103**(50), 18911–18916 (2006).
6. G. Giannone et al., "Dynamic superresolution imaging of endogenous proteins on living cells at ultra-high density," *Biophys. J.* **99**(4), 1303–1310 (2010).
7. B. Huang, H. Babcock, and X. Zhuang, "Breaking the diffraction barrier: super-resolution imaging of cells," *Cell* **143**(7), 1047–1058 (2010).
8. A. Chazeau et al., "Nanoscale segregation of actin nucleation and elongation factors determines dendritic spine protrusion," *EMBO J.* **33**(23), 2745–2764 (2014).
9. D. Nair et al., "Super-resolution imaging reveals that AMPA receptors inside synapses are dynamically organized in nanodomains regulated by PSD95," *J. Neurosci.* **33**(32), 13204–13224 (2013).
10. T. Vaithianathan et al., "Nanoscale dynamics of synaptic vesicle trafficking and fusion at the presynaptic active zone," *eLife* **5**, 1–14 (2016).
11. K. Perez de Arce et al., "Topographic mapping of the synaptic cleft into adhesive nanodomains," *Neuron* **88**(6), 1165–1172 (2015).
12. E. Hossy, C. Butler, and J. B. Sibarita, "Organization and dynamics of AMPA receptors inside synapses—nano-organization of AMPA receptors and main synaptic scaffolding proteins revealed by super-resolution imaging," *Curr. Opin. Chem. Biol.* **20**(1), 120–126 (2014).
13. T. C. Südhof, "Neuroigilins and neuexins link synaptic function to cognitive disease," *Nature* **455**(7215), 903–911 (2008).
14. M. A. Bemben et al., "The cellular and molecular landscape of neuroigilins," *Trends Neurosci.* **38**(8), 496–505 (2015).
15. G. J. Soler-Llavina et al., "The neuexin ligands, neuroigilins and leucine-rich repeat transmembrane proteins, perform convergent and divergent synaptic functions in vivo," *Proc. Natl. Acad. Sci. U. S. A.* **108**(40), 16502–16509 (2011).
16. K. H. Lim et al., "Stable, high-affinity streptavidin monomer for protein labeling and monovalent biotin detection," *Biotechnol. Bioeng.* **110**(1), 57–67 (2013).
17. M. Howarth et al., "Targeting quantum dots to surface proteins in living cells with biotin ligase," *Proc. Natl. Acad. Sci. U. S. A.* **102**(21), 7583–7588 (2005).
18. I. Chamma et al., "Mapping the dynamics and nanoscale organization of synaptic adhesion proteins using monomeric streptavidin," *Nat. Commun.* **7**, 10773 (2016).
19. C. Neupert et al., "Regulated dynamic trafficking of neuexins inside and outside of synaptic terminals," *J. Neurosci.* **35**(40), 13629–13647 (2015).
20. M. Missler et al., "Alpha-neuexins couple Ca<sup>2+</sup> channels to synaptic vesicle exocytosis," *Nature* **423**(6943), 939–948 (2003).
21. J. Ko et al., "LRRTM2 functions as a neuexin ligand in promoting excitatory synapse formation," *Neuron* **64**(6), 791–798 (2009).
22. D. Comoletti et al., "Characterization of the interaction of a recombinant soluble neuroigilin-1 with neuexin-1 $\beta$ ," *J. Biol. Chem.* **278**(50), 50497–50505 (2003).
23. T. J. Siddiqui et al., "LRRTMs and neuroigilins bind neuexins with a differential code to cooperate in glutamate synapse development," *J. Neurosci.* **30**(22), 7495–7506 (2010).
24. F. Levot et al., "SR-Tesseler: a method to segment and quantify localization-based super-resolution microscopy data," *Nat. Methods* **12**(11), 1065–1071 (2015).
25. D. S. Liu et al., "Quantum dot targeting with lipoic acid ligase and halotag for single-molecule imaging on living cells," *ACS Nano* **6**(12), 11080–11087 (2012).
26. J. de Wit et al., "LRRTM2 interacts with neuexin1 and regulates excitatory synapse formation," *Neuron* **64**(6), 799–806 (2009).
27. D. S. Liu et al., "Imaging trans-cellular neuexin-neuroigilin interactions by enzymatic probe ligation," *Plos One* **8**(2), e52823 (2013).
28. G. Giannone et al., "Neuexin-1 $\beta$  binding to neuroigilin-1 triggers the preferential recruitment of PSD-95 versus gephyrin through tyrosine phosphorylation of neuroigilin-1," *Cell Rep.* **3**(6), 1996–2007 (2013).
29. N. Uchida et al., "The catenin/cadherin adhesion system is localized in synaptic junctions bordering transmitter release zones," *J. Cell Biol.* **135**(3), 767–779 (1996).
30. P. Mendez et al., "N-cadherin mediates plasticity-induced long-term spine stabilization," *J. Cell Biol.* **189**(3), 589–600 (2010).
31. O. Bozdagi et al., "Increasing numbers of synaptic puncta during late-phase LTP: N-cadherin is synthesized, recruited to synaptic sites, and required for potentiation," *Neuron* **28**(1), 245–259 (2000).

32. H. D. MacGillavry et al., "Nanoscale scaffolding domains within the postsynaptic density concentrate synaptic AMPA receptors," *Neuron* **78**(4), 615–622 (2013).
33. R. T. Peixoto et al., "Transsynaptic signaling by activity-dependent cleavage of neuroligin-1," *Neuron* **76**(2), 396–409.(2012).
34. K. Suzuki et al., "Activity-dependent proteolytic cleavage of neuroligin-1," *Neuron* **76**(2), 410–422 (2012).
35. R. Galland et al., "3D high- and super-resolution imaging using single-objective SPIM," *Nat. Methods* **12**(7), 641–644 (2015).
36. K. H. Lim et al., "Engineered streptavidin monomer and dimer with improved stability and function," *Biochemistry* **50**(40), 8682–8691 (2011).
37. D. Demonte et al., "Structure-based engineering of streptavidin monomer with a reduced biotin dissociation rate," *Proteins* **81**(9), 1621–1633 (2013).
38. S. Kaech and G. Banker, "Culturing hippocampal neurons," *Nat. Protocol* **1**(5), 2406–2415 (2006).
39. A. Kechkar et al., "Real-time analysis and visualization for single-molecule based super-resolution microscopy," *Plos One* **8**(4), e62918 (2013).
40. I. Izeddin et al., "Wavelet analysis for single molecule localization microscopy," *Opt. Express* **20**, 2081–2095 (2012).

**Ingrid Chamma** is a postdoctoral fellow with the team of Olivier Thoumine in Bordeaux, France. She studied genetics and neuroscience at the University of Paris Diderot and received her PhD from the University Pierre and Marie Curie, Paris. Her current research focuses on the development of new molecular tools and their application to superresolution microscopy for protein targeting in complex microenvironments.

**Florian Leviet** studied computer sciences in Bordeaux, France. After a PhD at the LaBRI, he worked as a research engineer at the Bordeaux Imaging Center. He then joined the group of Jean-Baptiste Sibarita at the Interdisciplinary Institute for Neuroscience (IINS). His current research focuses on the development of new quantification and visualization methods for single-molecule localization microscopy, with a strong interest in geometric tessellations.

**Jean-Baptiste Sibarita** has a PhD thesis in physics and is expert in live cell microscopy and image processing and analysis. He has co-headed and developed the Cellular and Tissue Imaging Platform of the Institut Curie, Paris, for 12 years. Since 2009, he started his own group "Quantitative Imaging of the Cell" in the newly created Interdisciplinary Institute of Neuroscience, Bordeaux.

**Matthieu Sainlos** is a senior researcher at the French National Center for Scientific Research working at the IINS, Bordeaux, in the group of Daniel Choquet. His current research is focused on the use of multidisciplinary approaches from chemistry and protein engineering to imaging in order to develop tools and methods to investigate the molecular mechanisms of synaptic proteins. The strategies he develops include modulating protein interactions and monitoring specific proteins complexes.

**Olivier Thoumine** is team leader at IINS, Bordeaux. He is a biophysicist with a strong expertise in the mechanisms of cell adhesion. He has been using a combination of computer simulations, single-molecule imaging, and biomimetic assays to characterize molecular clutch mechanisms between the actin flow and N-cadherin adhesions in growth cones and dendritic filopodia, and to decipher the role of neuroligin/neuroligin complexes in synapse differentiation and function.